TRENDS IN SCIENCES 2025; 22(7): 9988
https://doi.org/10.48048/tis.2025.9988
RESEARCH ARTICLE

Photocatalytic Degradation of Congo Red Dye using $ZnFe_2O_4/SnO_2$ Composite with Response Surface Methodology (RSM) Optimization

Gierrald Abduh[1], Muhammad Said[2] and Poedji Loekitowati Hariani[2,*]

[1]Master Program in Chemistry, Faculty of Mathematics and Natural Sciences, Universitas Sriwijaya, Ogan Ilir 30662, Indonesia
[2]Research Group on Magnetic Materials, Department of Chemistry, Faculty of Mathematics and Natural Sciences, Universitas Sriwijaya, Ogan Ilir 30662, Indonesia

([*]Corresponding author's e-mail: puji_lukitowati@mipa.unsri.ac.id)

Received: 13 February 2025, Revised: 15 March 2025, Accepted: 22 March 2025, Published: 20 May 2024

Abstract

In this investigation, the synthesized $ZnFe_2O_4/SnO_2$ composites for the photocatalytic degradation of Congo red dye. Doping SnO_2 onto $ZnFe_2O_4$ optimized the energy gap, promoting light absorption in the visible spectrum. The $ZnFe_2O_4/SnO_2$ composites were analyzed using XRD, UV-DRS, SEM-EDS, VSM, and pHpzc. Photocatalytic degradation is optimized using Central Composite Design (CCD), which is based on response surface methodology (RSM). The XRD characterization results of the $ZnFe_2O_4/SnO_2$ composites demonstrate the success of the synthesis method. The composite has a combined 2θ of $ZnFe_2O_4$ and SnO_2, with a crystallite size of 17.50 nm. A band gap value of 2.46 eV indicates that the material can absorb most of the visible light spectrum. The EDS mapping results verify the presence of SnO_2 on the surface of $ZnFe_2O_4$, and the saturation magnetization value of 12.80 emu/g confirmed the composite's magnetic properties. Degradation optimization using RSM indicated that the quadratic model effectively characterizes the photocatalytic degradation of Congo red dye. The RSM model's high accuracy in predicting experimental outcomes is evidenced by the minor difference in efficiency degradation between experimental and predicted values, with an R^2 of 0.9851 and a *p*-value < 0.05. The optimum degradation efficiency was achieved at a solution pH of 4, a Congo red dye concentration of 10 mg/L, and an irradiation time of 80 min. The composite exhibits great stability, efficiency, and reliability; the reuse evaluation after 5 cycles indicated a deterioration reduction of less than 5 %.

Keywords: $ZnFe_2O_4/SnO_2$ composite, Degradation photocatalytic, Congo red dye, Optimization by RSM

Introduction

The rapid rate of population expansion, urbanization, and industrial development has heightened the demand for clean water [1,2]. Various sectors, including textiles, soap, cosmetics, paint, and paper, utilize dyes for coloration [3,4]. Inefficient operations in the textile industry led to around 10 - 20 % of dyes being discharged as liquid waste [5,6]. Liquid waste containing dyes is estimated to account for 20 % of global water contamination [6]. Humans and aquatic organisms are adversely affected by liquid waste that contains dyes. Dyes are stable chemicals that resist degradation; their presence in water can disrupt the photosynthesis of aquatic plants and phytoplankton, which are fundamental to the aquatic food chain, hence diminishing the oxygen supply in water [7,8]. The toxicity of dyes varies by kind, but generally, they can induce health issues, including carcinogenicity, mutagenicity, and respiratory tract illnesses [9]. Approximately 60 - 70 % of global dye produced consists of azo dyes, which are characterized by the presence of 1 or more chromophore groups (-N=N-) in their molecular structure [10,11]. Congo red dye ($C_{32}H_{22}N_6Na_2O_6S_2$) is a commonly utilized

industrial dye characterized by an aromatic ring and 2 azo groups.

The photocatalytic degradation approach for contaminant removal is frequently employed due to its efficiency, simplicity, and ability to transform toxins into simpler compounds without generating secondary pollutants [12]. The degradation process employs catalytic materials in conjunction with light sources, such ultraviolet, visible, or sunlight, to generate potent oxidative species [13]. Several metal oxides have been used for the photocatalytic degradation of dyes, including SnO_2 [14], TiO_2 [15], WO_3 [16], ZnO [17], CuO [18], and MnO_2 [19].

SnO_2 is an n-type semiconductor that is often used for the degradation of organic pollutants. Excellent chemical and thermal stability, non-toxicity, and low cost are the advantages of SnO_2 as a catalyst [20,21]. However, SnO_2 has a weakness, namely having a wide band gap of around 3.6 eV, suitable for absorbing light in the UV region, while sunlight only contains 5 % UV light. Another weakness is the high rate of electron-hole pair recombination, causing only a small portion of electrons and holes produced by light absorption to contribute to the catalytic reaction and separation process after being used for waste treatment [22,23]. To overcome these problems, several researchers have doped SnO_2 with several materials such as SnO_2-Cu [24], $SnO_2/NiFe_2O_4$ [23], Fe-SnO_2 [25], and Fe_3O_4-Ag/SnO_2 [26].

$ZnFe_2O_4$ is a ferrite compound with possible applications as a dopant for SnO_2. SnO_2 doped with $ZnFe_2O_4$ possesses a low band gap (~1.9 eV), enabling it to absorb light in the visible spectrum. UV and visible light can both be activated by $ZnFe_2O_4$. Moreover, $ZnFe_2O_4$ exhibits excellent chemical and thermal stability, is non-toxic, and possesses magnetic properties that enable the separation of catalysts from the reaction liquid via a magnetic attraction [27,28]. Recombination of electron-hole pairs is a prevalent issue in semiconductor photocatalysts. $ZnFe_2O_4$ can function as a superior center for charge carrier separation. Consequently, the amalgamation of $ZnFe_2O_4$ with SnO_2 constitutes a dependable approach to enhancing photocatalytic efficacy.

This research aims to carry out photocatalytic degradation of Congo red dye using $ZnFe_2O_4/SnO_2$ composites under visible radiation. Currently, a statistical approach to optimizing photocatalytic degradation is a method to maximize experimental efficiency and effectiveness. Response Surface Methodology (RSM) is an optimization modeling to analyze the influence between variables. This approach minimizes the number of experiments conducted, saving time and costs [29]. Through the combination of experiment and statistical optimization, this work offers novel and important insights into $ZnFe_2O_4$-SnO_2 composite for dye degradation since these contributions advance our understanding of wastewater treatment techniques. For $ZnFe_2O_4/SnO_2$ composite characterisation, XRD, SEM-EDS, UV-DRS, VSM, and pHpzc are employed. Optimization of photocatalytic degradation uses the RSM method with a Central Composite Design (CCD) design with the independent variables of pH, concentration and irradiation time.

Materials and methods

The chemicals used include $Zn(NO_3)_3$, $Fe(NO_3)_3.9H_2O$, $CO(NH_2)_2$, SnO_2, NaCl, HCl, NaOH, EDTA (Ethylenediaminetetraacetic acid), IPA (Isopropyl alcohol), BQ (Benzoquinone), and ethanol, which are analytical grade from Merck, Germany. Distilled water is used as a solvent.

Synthesis of $ZnFe_2O_4$

The synthesis of $ZnFe_2O_4$ was conducted by the solution combustion technique utilizing urea as the fuel source. A total of 1.72 g of $Zn(NO_3)_3$ and 6.70 g of $Fe(NO_3)_3.9H_2O$ were poured into a 100 mL beaker glass, then 3.96 mL of $CO(NH_2)_2$ and 50 mL of distilled water were added. The mixture was agitated for 30 min with a magnetic stirrer and subsequently dried in an oven at 80 °C for 10 h. Subsequently, calcination was conducted at a temperature of 500 °C for 2 h. The resultant black powder gained is $ZnFe_2O_4$.

Synthesis of $ZnFe_2O_4/SnO_2$ composite

The synthesis of the $ZnFe_2O_4/SnO_2$ composite was conducted with a mass ratio of $ZnFe_2O_4$ to SnO_2 equal to 1:2. A total of 1 g of $ZnFe_2O_4$ and 2 g of SnO_2 were ground together, and 50 mL of distilled water was added, then sonicated using a sonicator of 500 W for 30 min. The resultant brownish precipitate is a $ZnFe_2O_4/SnO_2$ composite, isolated from the solution and subsequently baked in an oven at 80 °C for 10 h. The

precipitate was calcined in solution at 500 °C for 3 h, with a heating rate of 4 °C/min.

Determination of pHpzc

pHpzc was determined following the methodology of Kumar *et al*. [30]. Zero point two g of $ZnFe_2O_4/SnO_2$ composite was introduced to multiple 100 mL conical flasks containing 50 mL of 0.1 M NaCl solution. The solution was modified to achieve a pH range of 2 to 12 with 0.1 M HCl and NaOH solutions. Additionally, agitation was performed with a shaker at a velocity of 120 rpm for 48 h. pHpzc was ascertained from the graph depicting initial pH against ΔpH ($pH_{final} - pH_{initial}$).

Characterization

A variety of techniques were employed for the characterization of $ZnFe_2O_4$ and $ZnFe_2O_4/SnO_2$ composites. Structural analysis was conducted using X-ray diffraction (XRD PANalycal) across the 2θ range of 10 - 90 °. Absorbance and band gap energy were assessed via Diffuse Reflectance Spectroscopy (DRS) utilizing a Cary 60 UV-Vis DRS apparatus. Material morphology, element composition, and element distribution were analyzed using a Scanning Electron Microscope (SEM) equipped with Dispersive Energy X-ray spectroscopy (EDS mapping) (SEM-EDS Hitachi Flexsem 100). The saturation magnetization was measured using a vibration sample magnetometer (VSM OXFORD 1.2 H) at a temperature of 298 K, within a magnetic field range of –18.0 to +18.0 kOe.

Design experiment by RSM

Response Surface Methodology (RSM) was employed in the experimental design utilizing Design Expert 13 software to optimize the degradation parameters. Central Composite Design (CCD) was used to investigate the correlation between independent factors and the response variable (degradation efficiency). The independent variables consist of solution pH (A), Congo red dye concentration (B), and irradiation time (C). A 300 W xenon lamp served as the irradiation source, positioned 15 cm from the sample. A total of 20 trials were conducted, each with 3 repetitions. A 50 mL solution of Congo red dye was prepared by incorporating 0.02 g of the $ZnFe_2O_4/SnO_2$ combination. The experiment configuration is detailed in **Table 1**. To establish an adsorption/desorption equilibrium, stirring was conducted in a dark environment for 30 min prior to the photocatalytic degradation process. The absorbance of the Congo red dye solution was quantified at a wavelength of 498 nm. The efficiency of deterioration was ascertained using the subsequent equation:

$$Degradation\ (\%) = \frac{C_0 - C}{C_0} \times 100 \quad (1)$$

Where C_0 dan C represent the initial and final concentration of Congo red dye.

Table 1 Independent value for CCD.

Factor	Unit	1–	0	+1
A: pH solution		4	7	10
B: Dye concentration	mg/L	10	20	30
C: Irradiation time	Min	20	50	80

Results and discussion

Characterization of $ZnFe_2O_4$ and $ZnFe_2O_4/SnO_2$ composite

Figure 1 illustrates the diffraction peaks of $ZnFe_2O_4$ and the $ZnFe_2O_4/SnO_2$ composite. The $ZnFe_2O_4$ peak aligns with JCPDS card 22-1012, indicating a cubic spinel structure for $ZnFe_2O_4$ [31]. The spinel structure comprises Zn^{2+} cations typically residing in tetrahedral sites (A-site) and Fe^{3+} cations in octahedral sites (B-site) within the oxide lattice. The 2θ peaks observed at 18.30, 30.03, 35.42, 43.08, 53.11, 56.90, and 62.55 ° correspond to Miller indices (111), (220), (311), (400), (422), (511), and (440). The peak of the $ZnFe_2O_4/SnO_2$ composite comprises the combination of 2 distinct peaks: $ZnFe_2O_4$ and SnO_2. SnO_2 exhibits peaks at 2θ = 26.60, 34.04, 37.91, 51.76, 54.76, 64.73, and 65.88 °. According to JCPDS card No. 41-1445, the peaks that have been detected match the crystal planes (110), (101), (200), (211), (220), (112), and (301). The Scherrer equation is employed to

ascertain crystallite size. The crystallite size of $ZnFe_2O_4$ is 21.23 nm, whereas the $ZnFe_2O_4/SnO_2$ composite exhibits a crystallite size of 17.50 nm. Doping SnO_2 with $ZnFe_2O_4$ leads to smaller crystal sizes because the interface or strain in the lattice limits their growth.

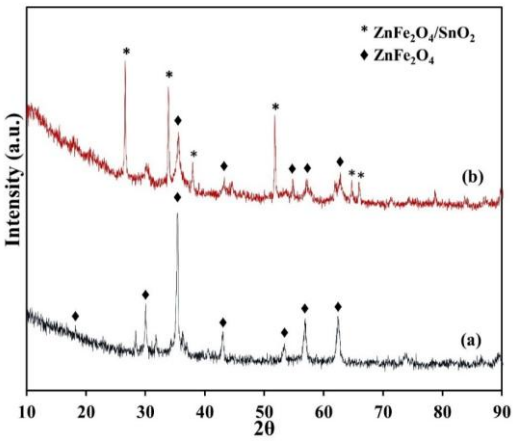

Figure 1 XRD pattern of (a) $ZnFe_2O_4$ and (b) $ZnFe_2O_4/SnO_2$ composite.

The SnO_2 peak in the UV-DRS spectra typically manifests in the ultraviolet range. The investigation conducted by Desouky *et al.* [23] determined the wavelength of SnO_2 to be 330 nm. The combination with $NiFe_2O_4$ induces a shift in the wavelength within the visible spectrum, approximately at 600 nm. This investigation suggests that the absorption peak of $ZnFe_2O_4/SnO_2$ occurs at 550 nm (**Figure 2(a)**). The band gap is an essential indicator that signifies the optical qualities and prospective applications of composites in photocatalysis. $ZnFe_2O_4$ is an n-type semiconductor with a low band gap (1.7 - 2.2 eV), whereas SnO_2 possesses a broad band gap (~3.6 eV) [25,32]. Charge transfer at the contact can diminish the energy necessary for electron excitation. The combined effect of $ZnFe_2O_4$ with SnO_2 can diminish the band gap of SnO_2. **Figure 2(b)** shows that the band gap of $ZnFe_2O_4$ is 1.98 eV, while that of the $ZnFe_2O_4/SnO_2$ combination is 2.46 eV. The findings align with other research, specifically indicating that the band gap value of $ZnFe_2O_4$ ranges from 1.89 to 1.92 eV when synthesized via the solution combustion method at temperatures between 400 and 1000 °C [27], whereas $ZnFe_2O_4$ synthesized through the laser ablation method exhibits a band gap between 2.17 and 2.27 eV [33].

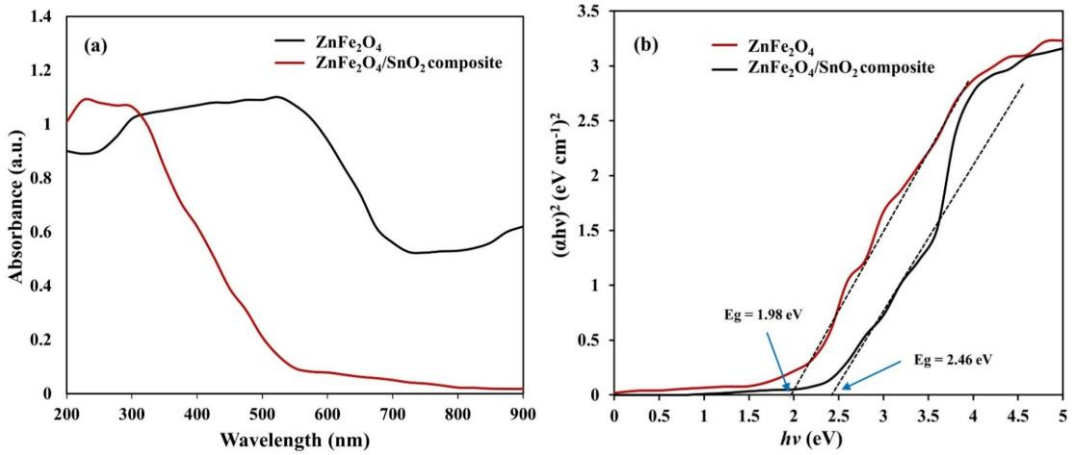

Figure 2 (a) UV DRS absorption spectra and (b) Plot of $(\alpha h\upsilon)^2$ against $h\upsilon$ of $ZnFe_2O_4$ and $ZnFe_2O_4/SnO_2$ composite.

Figure 3 illustrates the morphology of $ZnFe_2O_4$ and $ZnFe_2O_4/SnO_2$ composites as observed through SEM investigation. The features of the $ZnFe_2O_4/SnO_2$ composite showed a reduction in the size of the fibrillar structure and sporadic breakdown in the fibrillar structure into individualised fibrils, whereas the composite was embedded with SnO_2. The EDS mapping results depicted in **Figure 4** indicate that the composition of $ZnFe_2O_4/SnO_2$ comprises the elements O, Sn, Zn, and Fe. The presence of Sn signifies the successful synthesis of the $ZnFe_2O_4/SnO_2$ compound.

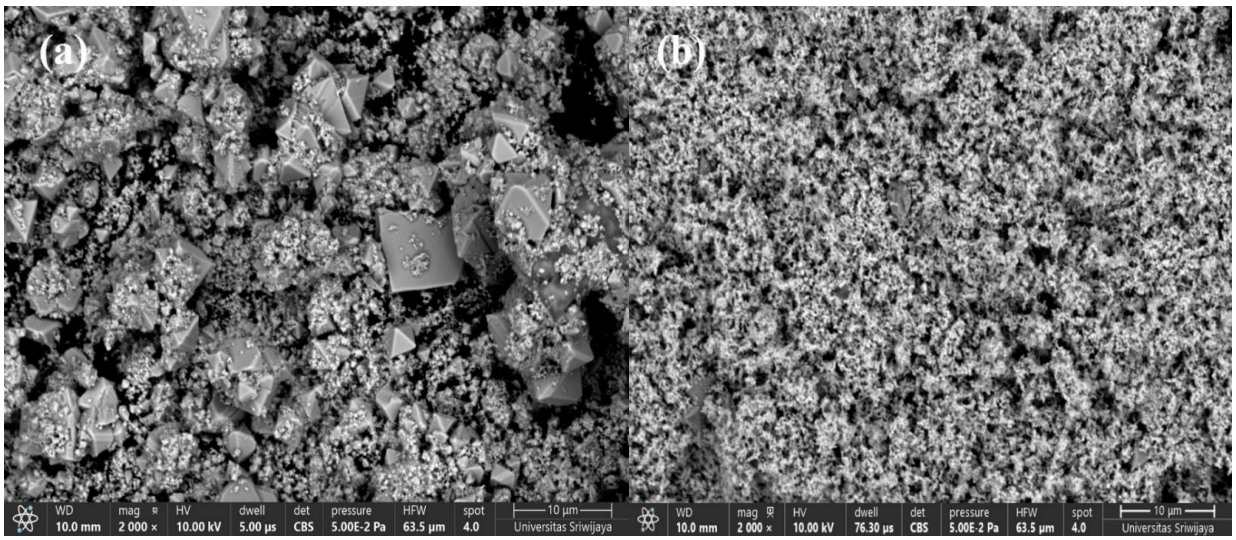

Figure 3 Morphology of (a) $ZnFe_2O_4$ and (b) $ZnFe_2O_4/SnO_2$ composite.

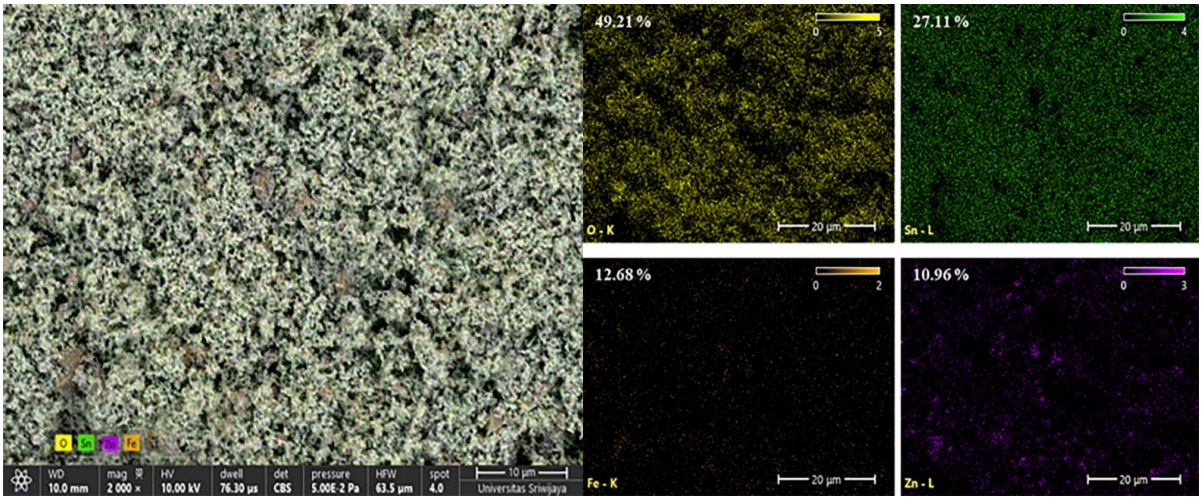

Figure 4 Elemental mapping of $ZnFe_2O_4/SnO_2$ composite.

The synthesis method and particle size influence the magnetic characteristics of $ZnFe_2O_4$. The ferrimagnetic characteristics of $ZnFe_2O_4$ arise from the perturbation of the arrangement of Fe^{3+} and Zn^{2+} ions at the tetrahedral (A) and octahedral (B) sites. This study determined the saturation magnetization (Ms) value of $ZnFe_2O_4$ to be 28.15 emu/g. The Ms value acquired in this investigation exceeded the findings of prior studies, specifically ± 10 emu/g [34] and 11.04 nm [35]. The $ZnFe_2O_4/SnO_2$ composite exhibits a Ms value of 12.80 emu/g. The reduction in the Ms value of the composite results from doping with SnO_2, which is diamagnetic. The investigation conducted by Chen *et al*. [36] revealed a similar occurrence, wherein the Ms value of $ZnFe_2O_4$, initially 44 emu/g, decreased to 11 emu/g upon doping with TiO_2. Despite the reduction in magnetic properties, the composite continues to exhibit robust magnetic characteristics (**Figure 5**).

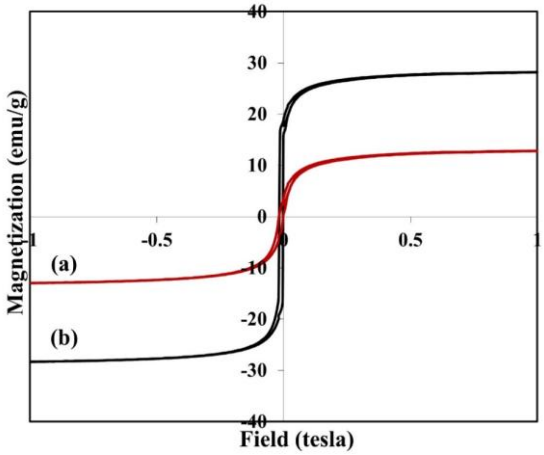

Figure 5 Magnetization curves of (a) $ZnFe_2O_4$ and (b) $ZnFe_2O_4/SnO_2$ composite at room temperature.

The surface of a material can be positively or negatively charged depending on the pH of the solution. The pH of 0 charge (pHpzc) is the pH value on the surface of a material where the number of positive and negative charges adsorbed on the surface of the material is balanced. The pHpzc for the $ZnFe_2O_4/SnO_2$ composite is 6.70, indicating that at this pH, the material's surface is neutral, and ions from the solution will not be significantly adsorbed. At a pH below 6.70, the $ZnFe_2O_4/SnO_2$ composite is likely to have a positive charge due to the adsorption of protons (H^+) on its surface. Conversely, with a pH exceeding 6.70, this substance will acquire a negative charge owing to a reduction in H^+ ion concentration and an elevation in OH^- ion concentration in the solution. This value closely aligns with other studies, specifically the pHpzc of the $ZnFe_2O_4/Mn_2O_4$ composite, which is 6.75. **Figure 6** illustrates the pHpzc curve of the $ZnFe_2O_4/SnO_2$ composite.

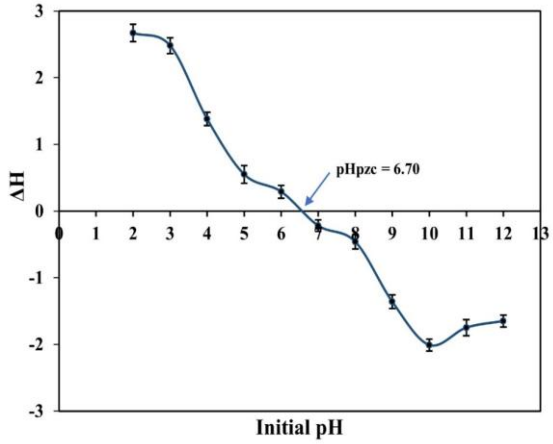

Figure 6 pHpzc of $ZnFe_2O_4/SnO_2$ composite.

Photocatalytic degradation using RSM

The photocatalytic degradation experiment was designed using RSM based on CCD to investigate the influence of independent factors on the degradation efficiency of Congo red dye. RSM is based on a nonlinear multivariate model that employs an experimental design yielding enough response data to derive the most suitable mathematical model for the experiment [29]. The independent variables are solution pH (A), Congo red dye concentration (B), and irradiation time (B). **Table 2** presents the degradation efficiency of the experimental data and forecasts for Congo red dye under visible light irradiation.

Table 2 Congo red dye degradation efficiency (%) based on experiments and predicted.

Run	Variables independent			Degradation (%)	
	A	B	C	Experiment	Predicted
1	7	20	50	67.42	67.15
2	7	20	50	67.80	67.15
3	7	20	50	69.31	67.15
4	4	30	80	96.72	92.82
5	7	10	50	69.69	72.41
6	4	30	20	68.69	68.52
7	4	20	50	84.09	83.75
8	7	10	50	73.48	72.41
9	7	20	20	63.26	64.57
10	7	20	50	64.39	67.15
11	10	30	80	59.59	59.29
12	7	20	80	74.62	74.58
13	7	30	50	56.57	55.68
14	10	10	80	66.67	66.53
15	7	20	50	69.32	67.15
16	4	30	80	71.72	72.82
17	10	10	20	51.52	50.81
18	10	20	50	53.41	55.02
19	10	30	20	40.40	40.68
20	10	10	20	51.52	50.81

The results of ANOVA analysis of 20 experiments are presented in **Table 3** to assess the suitability of the model. A p-value of < 0.05 signifies that the established quadratic model is statistically significant and suitable for predicting the efficacy of Congo red dye degradation. The 3 independent variables, pH (A), dye concentration (B), and irradiation time (C), exhibit p-values < 0.05, signifying their influence on degradation efficiency. The interactions between variables that do not affect one another are BC and C^2. The Lack of Fit score is not significant (p-value > 0.05), indicating that the quadratic model adequately represents the connection between the variables [37].

Table 3 ANOVA analysis for degradation photocatalytic of Congo red dye.

Source	Sum of square	df	Mean square	*F*-value	*p*-value	
Model	3150.58	9	350.06	73.63	< 0.0001	Significant
A: pH	1337.47	1	1337.47	281.31	< 0.0001	
B: Concentration	54.69	1	54.69	11.50	0.0069	
C: Irradiation time	56.84	1	56.84	11.96	0.0061	
AB	75.83	1	75.83	15.95	0.0025	
AC	114.84	1	114.84	24.15	0.0006	
BC	5.51	1	5.51	1.16	0.3070	
A^2	64.24	1	64.24	13.51	0.0043	

Source	Sum of square	df	Mean square	*F*-value	*p*-value	
B^2	43.23	1	43.23	9.09	0.0130	
C^2	8.65	1	8.65	1.82	0.2072	
Residual	47.54	10	4.75			
Lack of Fit	22.09	4	5.52	1.30	0.3674	Not significant
Pure error	25.46	6	4.24			
Cor Total	3198.13	19				

The coefficient of determination is close to 1 (R^2 = 0.9851), signifying a strong correlation between observed and predicted values (**Table 4**). Adjusted R^2 pertains to model performance, whereas predicted R^2 evaluates the model's prediction capability on novel data. A disparity of less than 0.2 between adjusted R^2 and predicted R^2 values signifies commendable performance [38]. Adeq precision is used to evaluate the signal-to-noise ratio in the model. A precision number of 4 is preferable, indicating sufficient predictive capability.

Table 4 Fit statistic model for photocatalytic degradation of Congo red dye.

Std. Dev	2.18	R^2	0.9851
Mean	66.66	Adjusted R^2	0.9718
C.V. %	3.27	Predicted R^2	0.9259
		Adeq Precision	37.1110

The model's validity can be assessed by the normal distribution of the residuals and the graphs comparing predicted and experimental values. If the points on the graph align along a straight line (approaching the diagonal), the residuals are deemed to be normally distributed. Substantial divergences from this line suggest that the model fails to forecast accurately for certain data. **Figure 7** illustrates a random distribution of data around the diagonal line, suggesting that the employed model predicts the response with considerable accuracy.

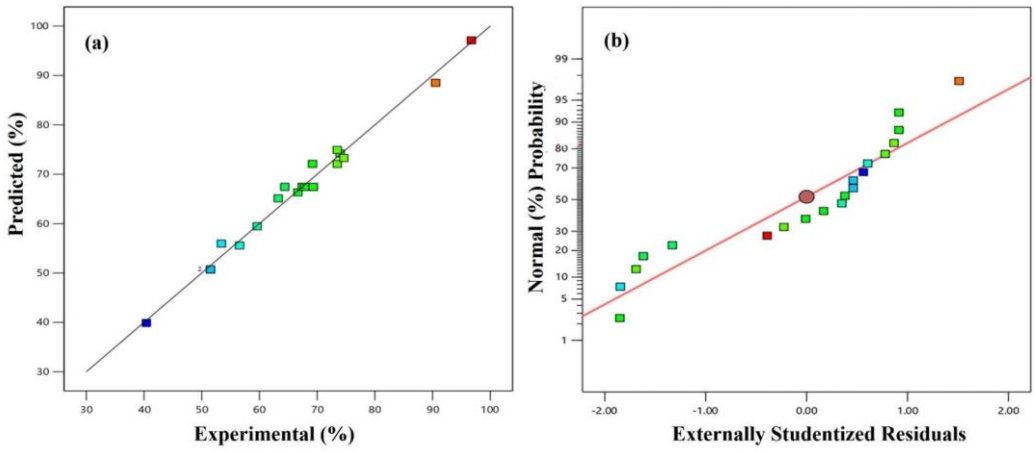

Figure 7 (a) The graphical plot of predicted versus experimental and (b) the normal probability plot.

The following is an expression for a quadratic model that explains the relationship between variables:

Degradation (%) = (171.19532 – 18.0455A – 0.442865B - 0.492599C + 0.127759AB + 0.052407AC +

$0.003324BC + 0.531825A^2 - 0.036092B^2 + 0.001951C^2)$ (2)

Figure 8 shows the contour plot and 3D surface response. This diagram illustrates the correlation between 3 independent factors and the response variable [39]. The 3D surface response demonstrates the variation of the response variable in relation to the interplay of 2 independent variables. The degradation efficiency is calculated by identifying the independent variable value that yields the optimal result. The degradation efficiency increases with decreasing pH and concentration, as evidenced by the red hue. The $ZnFe_2O_4/SnO_2$ composite possesses a pHpzc of 6.70, indicating that it is positively charged at solution pH values below this threshold. Electrostatic attractive interactions arise due to the anionic nature of Congo red dye, namely the ionization of the negatively charged sulfate group [22]. At elevated pH, the $ZnFe_2O_4/SnO_2$ composite combination exhibits a negative surface charge, which repels the negatively charged Congo red dye molecules. Additional research indicates that the degradation efficiency of Congo red is maximized at acidic pH levels [3,40].

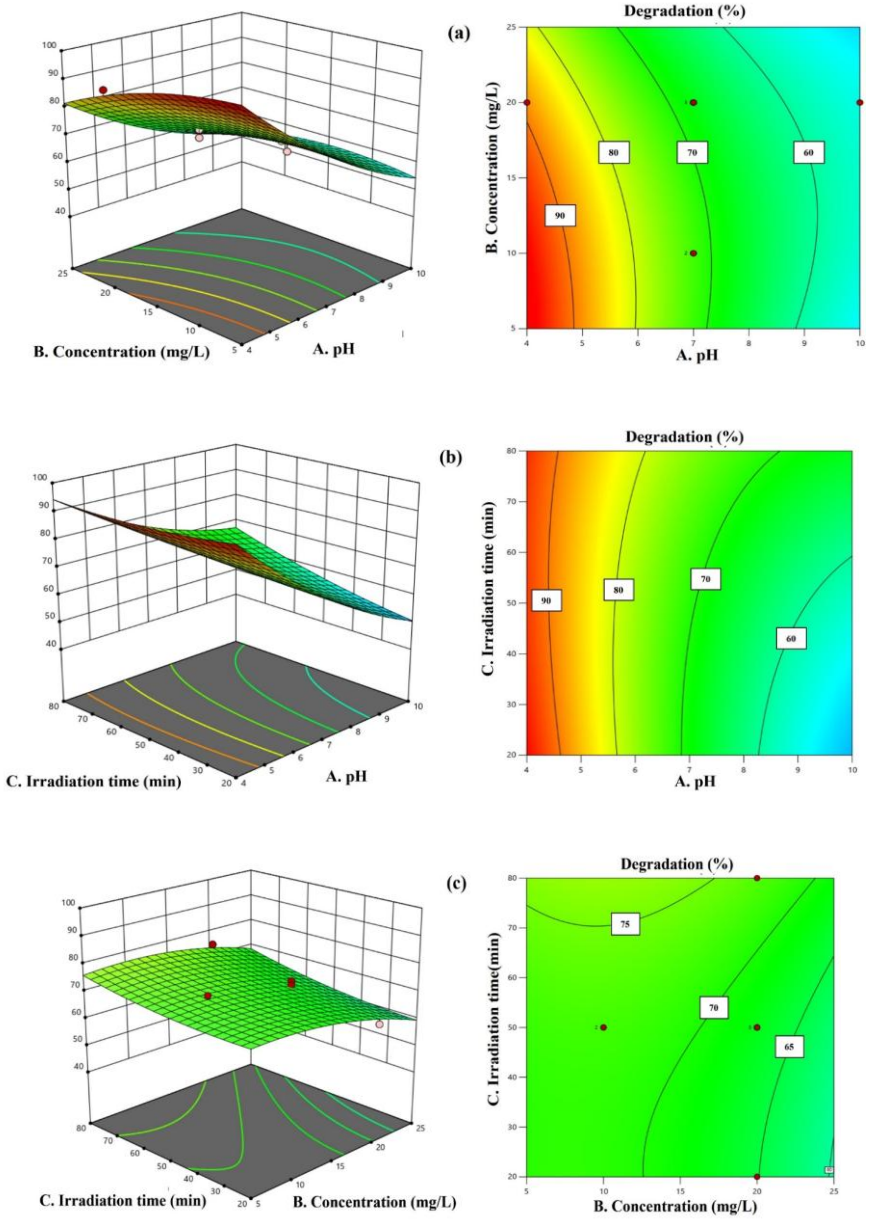

Figure 8 3D surface and contour plot degradation photocatalytic of Congo red dye.

The efficacy of the photocatalytic degradation process is enhanced when the dye is uniformly distributed throughout the composite. Elevated dye concentrations inhibit the composite's ability to absorb irradiation [41]. The degradation efficiency is higher at low concentrations. Extended irradiation correlates with increased deterioration efficiency, as the semiconductor absorbs a greater amount of light energy. When a semiconductor is exposed to light with enough energy, electrons from the valence band (VB) move to the conduction band (CB), creating electron-hole pairs (e^-/h^+). Electrons (e^-) in the conduction band and holes (h^+) in the valence band are crucial for the generation of reactive species [42].

To ensure that the predictive model generated from the RSM analysis is in accordance with the actual conditions, confirmation is needed. Confirmation is done by conducting additional experiments at optimum conditions and then comparing the experimental results with the model predictions. The recommended conditions, with a desirability of 1, include a pH of 4, a Congo red dye concentration of 10 mg/L, and an irradiation time of 80 min (**Table 5**). The predicted results were 97.10 % while the observed value was 96.12 %. The very small difference of degradation efficiency and in the range of the Prediction Interval (PI) Low and PI High indicates that the RSM model has a fairly accurate prediction. The study found that the degradation efficiency was better than in several other studies on Congo red dyes. Specifically, it reached 91.67 % with Pani@rGO/CuO and 93.77 % with rGO/Ag@ZnO [43,44].

Table 5 Validation of optimum conditions for photocatalytic degradation of Congo red dye.

Parameter	Predicted value	Observed value	Std. Dev	95 % PI low	95 % PI high
Degradation (%)	97.10	96.12	2.18	91.54	102.67

Scavenger study

The scavenger study is employed to investigate the active species and the mechanism of electron transfer. The investigation utilized EDTA, BQ, and IPA. These 3 chemicals were added prior to the photocatalytic degradation of Congo red dye utilizing the $ZnFe_2O_4/SnO_2$ composite. The degradation mechanism was determined through the scavenger, which resulted in a substantial reduction in degradation efficiency. **Figure 9** demonstrates that the $ZnFe_2O_4/SnO_2$ composite broke down 96.12 % of dye when no scavenger was used. However, when IPA, EDTA, and BQ were added, the breakdown degradation dropped to 72.56, 41.3, and 32.45 %, respectively. The results show that the main agents breaking down Congo red dye are BQ, especially superoxide radicals ($\bullet O_2^-$), followed by hydroxyl radicals ($\bullet OH^-$) and holes (h^+). Many studies show that superoxide radicals play an important role in breaking down substances, such as the Methylene blue dye when using Cu-doped α-MnO_2 [45] and the dye Congo red dye with Gd_2O_3 on g-C_3N_4 [46].

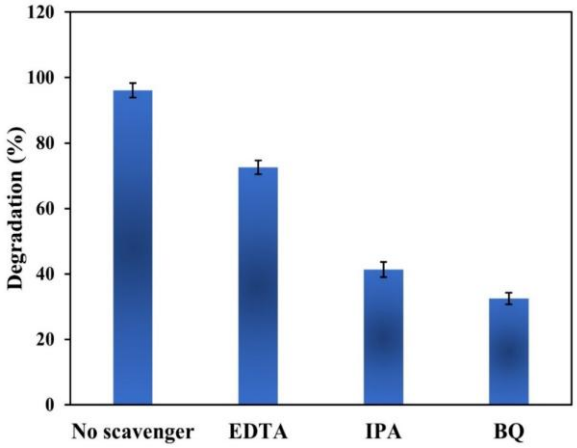

Figure 9 Experiments on trapping reactive species for $ZnFe_2O_4/SnO_2$ composite.

Recyclability study

The reusability of $ZnFe_2O_4/SnO_2$ composites is very important in cost-effectiveness, particularly when these composites are applied in industrial or environmental processes. To reuse $ZnFe_2O_4/SnO_2$, after the composite is used for photocatalytic degradation, it is separated from the solution using centrifugation. The composite is washed using distilled water and ethanol, followed by drying using an oven at a temperature of 80 °C for 2 h. The composite is reused for photocatalytic degradation of Congo red dye. The same work is carried out for 5 cycles. The degradation efficiency of 5 cycles is 95.23, 94.43, 93.51, 91.89, and 90.27 %. The decrease in degradation efficiency for each additional cycle shows that it is getting bigger, with an average decrease for each cycle of 1.2575 % (**Figure 10**). The loss of catalyst weight in subsequent cycles due to washing and drying may cause this phenomenon [47]. However, the $ZnFe_2O_4/SnO_2$ composite shows good performance because during 5 cycles, there is a decrease in degradation efficiency of only 4.96 %. This performance is better than the CoO-ZnO nanocomposite catalyst, which has a degradation efficiency reduction of 12.35 % in 5 cycles and 2.47 % in each cycle for the photocatalytic degradation of Methyl red dye [37]. The ability of composites to be reused effectively is an advantage because it minimizes costs in waste processing.

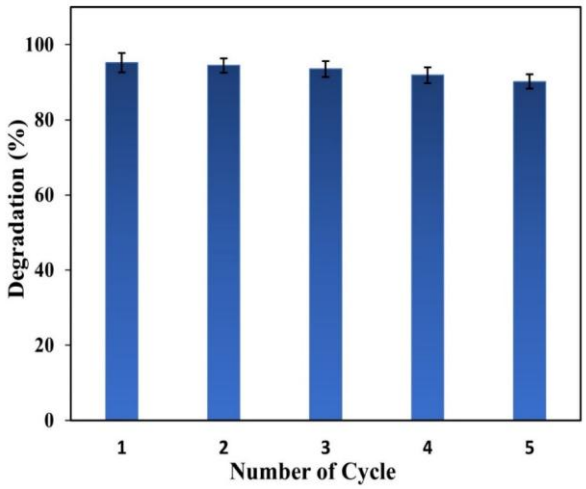

Figure 10 The cycling degradation of $ZnFe_2O_4/SnO_2$ composite.

Conclusions

$ZnFe_2O_4/SnO_2$ composite has been produced successfully with a mass ratio of $ZnFe_2O_4$ to SnO_2 of 1:2. The composite has magnetic features, a crystallite size of 17.50 nm, a saturation magnetization of 12.80 emu/g, and a band gap of 2.46 eV, which allows it to absorb visible light. A statistical study employing RSM with CCD yields a quadratic mathematical equation (*p*-value < 0.05, $R^2 = 0.9851$) that effectively characterizes the interaction among 3 independent variables. The best photocatalytic degradation was achieved at a pH of 4, a concentration of Congo red dye of 10 mg/L, and an irradiation time of 80 min. The reactive species involved in photocatalytic degradation are superoxide anion radicals ($\bullet O_2^-$). The catalyst has excellent stability, and the composite can be regenerated, with a degrading efficiency reduction of less than 5 % after up to 5 cycles. Consequently, the $ZnFe_2O_4/SnO_2$ composite holds significant potential for large-scale wastewater treatment applications.

Acknowledgements

The authors are grateful to the Directorate General of Higher Education, Research and Technology for the Tesis Magister scheme for the 2024 fiscal year, which is governed by contract number 090/E5/PG.02.00.PL/2024.

References

[1] T Zobeidi, J Yaghoubi and M Yazdanpanah. Developing a paradigm model for the analysis of farmers' adaptation to water scarcity. *Environment, Development and Sustainability* 2022; **24(4)**, 5400-5425.

[2] A Dehghani, S Baradaran and S Movahedirad. Synergistic degradation of Congo Red by hybrid advanced oxidation via ultraviolet light, persulfate, and hydrodynamic cavitation. *Ecotoxicology and Environmental Safety* 2024; **272**, 116042.

[3] SE Bourachdi, F Moussaoui, AR Ayub, AE Amri, FE Ouadrhiri, A Adachi, A Bendaoud, AM Idrissi and A Lahkimi. DFT theoretical analysis, experimental approach, and RSM process to understand the congo red adsorption mechanism on Chitosan@Graphene oxide beads. *Journal of Molecular Structure* 2025; **1321(4)**, 140090.

[4] Y Yang, N Ali, A Khan, S Khan, S Khan, H Khan, S Xiaoqi, W Ahmad, S Uddin, N Ali and M Bilal. Chitosan-capped ternary metal selenide nanocatalysts for efficient degradation of Congo red dye in sunlight irradiation. *International Journal of Biological Macromolecules* 2021; **167**, 169-181.

[5] AJ Sayyed, DV Pinjari, SH Sonawane, BA Bhanvase, J Sheikh and M Sillanpää. Cellulose-based nanomaterials for water and wastewater treatments: A review. *Journal of Environmental Chemical Engineering* 2021; **9(6)**, 106626.

[6] D Gautam, S Kumari, B Ram, GS Chauhan and K Chauhan. A new hemicellulose-based adsorbent for malachite green. *Journal of Environmental Chemical Engineering* 2018; **6(4)**, 3889-3897.

[7] N Yahya, F Aziz, NA Jamaludin, MA Mutalib, AF Ismail, WNW Salleh, J Jaafar, N Yusof and NA Ludin. A review of integrated photocatalyst adsorbents for wastewater treatment. *Journal of Environmental Chemical Engineering* 2018; **6(6)**, 7411-7425.

[8] R Javaid and UY Qazi. Catalytic oxidation process for the degradation of synthetic dyes: An overview. *International Journal of Environmental Research and Public Health* 2019; **16(11)**, 2066.

[9] AYL Tang, CKY Lo and C Kan. Textile dyes and human health: A systematic and citation network analysis review. *Coloration Technology* 2018; **134(4)**, 245-257.

[10] K Balapure, N Bhatt and D Madamwar. Mineralization of reactive azo dyes present in simulated textile waste water using down flow microaerophilic fixed film bioreactor. *Bioresource Technology* 2015; **175(1)**, 1-7.

[11] BL Alderete, JD Silva, R Godoi, FRD Silva, SR Taffarel, LPD Silva, ALH Garcia HM Júnior, HLND Amorim and JN Picada. Evaluation of toxicity and mutagenicity of a synthetic effluent containing azo dye after Advanced Oxidation Process treatment. *Chemosphere* 2021; **263**, 128291.

[12] A Farhan, J Arshad, EU Rashid, H Ahmad, S Nawaz, J Munawar, J Zdarta, T Jesionowski and M Bilal. Metal ferrites-based nanocomposites and nanohybrids for photocatalytic water treatment and electrocatalytic water splitting. *Chemosphere* 2023; **310**, 136835.

[13] OMA Halim, NH Mustapha, SNM Fudzi, R Azhar, NIN Zanal, NF Nazua, AH Nordin, MSM Azami, MAM Ishak, WINW Ismail and Z Ahmad. A review on modified ZnO for the effective degradation of methylene blue and rhodamine B. *Results in Surfaces and Interfaces* 2025; **18**, 100408.

[14] C Sun, J Yang, M Xu, Y Cui, W Ren, J Zhang, H Zhao and B Liang. Recent intensification strategies of SnO_2-based photocatalysts: A review. *Chemical Engineering Journal* 2022; **427**, 131564.

[15] Q Li, T Zhao, M Li, W Li, B Yang, D Qin, K Lv, X Wang, L Wu, X Wu and J Sun. One-step construction of Pickering emulsion via commercial TiO_2 nanoparticles for photocatalytic dye degradation. *Applied Catalysis B: Environment and Energy* 2019; **249**, 1-8.

[16] S Yao, F Qu, G Wang and X Wu. Facile hydrothermal synthesis of WO_3 nanorods for photocatalysts and supercapacitors. *Journal of Alloys and Compounds* 2017; **724**, 695-702.

[17] AB Siddique, MA Shaheen, A Abbas, Y Zaman, MA Bratty, A Najmi, A Hanbashi, M Mustaqeem, HA Alhazmi, ZU Rehman, K Zoghebi and HMA Amin. Thermodynamic and kinetic insights into azo dyes photocatalytic degradation on

biogenically synthesized ZnO nanoparticles and their antibacterial potential. *Heliyo*n 2024; **10(23)**, e40679.

[18] SB Sharafudheen, C Vijayakumar, R Rajakrishnan, A Alfarhan, S Arokiyaraj and MR Bindhu. Biogenic synthesis of porous CuO nanoparticles: Synergistic effects in photocatalytic dye degradation and electrochemical energy storage applications. *Journal of Crystal Growth* 2025; **649**, 127917.

[19] M Khatri, A Gupta, K Gyawali, A Adhikari, AR Koirala and N Parajuli. Photocatalytic degradation of dyes using synthesized δ-MnO_2 nanostructures. *Chemical Data Collections* 2022; **39**, 100854.

[20] AM Al-Hamdi, U Rinner and MSillanpa. Tin dioxide as a photocatalyst for water treatment: A review. *Process Safety and Environmental Protection* 2017; **107**, 190-205.

[21] V Perumal, A Sabarinathan, M Chandrasekar, M Suvabsh, C Inmozhi, R Uthrakumar, AB Isaev, A Raja, MS Elshikh, SM Almutairia and K Kaviyarasu. Hierarchical nanorods of graphene oxide decorated SnO_2 with high photocatalytic performance for energy conversion applications. *Fuel* 2022; **324**, 124599.

[22] Z Yang, L Lv, Y Dai, Z Xv and D Qian. Synthesis of ZnO-SnO_2 composite oxides by CTAB-assisted co-precipitation and photocatalytic properties. *Applied Surface Science* 2010; **256(9)**, 2898-2902.

[23] FGE Desouky, MM Saadeldin, MA Mahdy and IKE Zawawi. Tuning the structure, morphological variations, optical and magnetic properties of SnO_2/$NiFe_2O_4$ nanocomposites for promising applications. *Vacuum* 2021; **185**, 110003.

[24] M Arif, MZU Shah, SA Ahmad, MS Shah, Z Ali, A Ullah, M Idrees, J Zeb, P Song, T Huang and J Yi. High photocatalytic performance of copper-doped SnO_2 nanoparticles in degradation of Rhodamine B dye. *Optical Materials* 2022; **134**, 113135.

[25] MHDS Ribeiro, GN Marques, AJ Moreira, MM Oliveira, RC Oliveira, RTD Silva, AC Krohling, WAA Macedo, MIB Bernardi, LH Mascaro, JHG Rangel and HBD Carvalho. Green-assisted synthesis of highly defective nanostructured Fe-doped SnO_2: Magnetic and photocatalytic properties evaluation. *Acta Materialia* 2024; **277**, 120194.

[26] BS Shagolsem and NM Singh. Ternary photocatalyst of Fe_3O_4/Ag-SnO_2 with *Parkia speciosa* extract improves visible-light-driven photocatalytic degradation of dye. *Inorganic Chemistry Communications* 2024; **162**, 112245.

[27] TP Oliveira, GN Marques, MAM Castro, RCV Costa, JHG Rangel, SF Rodrigues, CCD Santos and MM Oliveira. Synthesis and photocatalytic investigation of $ZnFe_2O_4$ in the degradation of organic dyes under visible light. *Journal of Materials Research Technology* 2020; **9(6)**, 15001-15015.

[28] CG Anchieta, EC Severo, C Rigo, MA Mazutti, RC Kuhn, EI Muller, EMM Flores, RFPM Moreira and EL Foletto. Rapid and facile preparation of zinc ferrite ($ZnFe_2O_4$) oxide by microwave-solvothermal technique and its catalytic activity in heterogeneous photo-Fenton reaction. *Materials Chemistry and Physics* 2015; **160**, 141-147.

[29] R Moeinzadeh, N Azizi, M Hekmati, M Qomi and D Esmaeili. ZnONPs/covalent triazine frameworks nanocomposite as high-performance photocatalysts for degradation of Congo red under visible light. *Materials Chemistry and Physics* 2023; **307**, 128122.

[30] N Kumar, MR Ansari, S Khaladkar, O Maurya, KR Peta, A Kalekar, MK Singha and JK Dash. $NiFe_2O_4$ nanoparticles as highly efficient catalyst for oxygen reduction reaction and energy storage in supercapacitor. *Materials Chemistry and Physics* 2024; **316**, 129072.

[31] R Li, H Hu, Y Ma, X Liu, L Zhang, S Zhou, B Deng, H Lin and H Zhang. Persulfate enhanced photocatalytic degradation of bisphenol A over wasted batteries-derived $ZnFe_2O_4$ under visible light. *Journal of Cleaner Production* 2020; **276**, 124246.

[32] FU Zaman, A Kumar, G Yasin, FO Boakye, F Muhammad, S Iqbal, KM Alotaibi, L Hou and C Yuan. Enhanced photocatalytic degradation of organic dyes by carbon quantum dots-$ZnFe_2O_4$ composites. *Journal of Alloys and Compounds* 2024; **983**, 173860.

[33] JS Duque, BM Madrigal, H Riascos and YP Avila. Colloidal metal oxide nanoparticles prepared by laser ablation technique and their antibacterial test. *Colloids and Interfaces* 2019; **3(1)**, 25.

[34] FS Volkov, MA Kamenskii, LA Voskanyan, NP Bobrysheva, OM Osmolovskaya and SN Eliseeva. Impact of $ZnFe_2O_4$ nanoparticles parameters on magnetic and electrochemical performance. *Materialia* 2024; **34**, 102046.

[35] PA Vinosha, LA Mely, JE Jeronsia, S Krishnan and SJ Das. Synthesis and properties of spinel $ZnFe_2O_4$ nanoparticles by facile co-precipitation route. *Optik* 2017; **134**, 99-108.

[36] R Chen, S Ding, B Wang and X Ren. Preparation of $ZnFe_2O_4$@TiO_2 novel core-shell photocatalyst by ultrasonic method and its photocatalytic degradation activity. *Coatings* 2022; **12(10)**, 1407.

[37] M Afaq, A Sajid, Q Manzoor, F Imtiaz, A Sajid, R Javed, A Ahmad, N Alwadai, W Mnif and M Iqbal. Sonochemical synthesis of CoO-ZnO nanocomposite and optimizing the degradation of toxic anionic dye using RSM-BBD. *Materials Science and Engineering: B* 2025; **312**, 117847.

[38] L Aeindartehran and SSA Talesh. Enhanced photocatalytic degradation of Acid Blue 1 using Ni-Decorated ZnO NPs synthesized by sol-gel method: RSM optimization approach. *Ceramics International* 2021; **47(19)**, 27294-27304.

[39] S Hmamouchi, AE Yacoubi, ME Hezzat, B Sallek and BCE Idrissi. Optimization of photocatalytic parameters for MB degradation by g-C_3N_4 nanoparticles using Response Surface Methodology (RSM). *Diamond and Related Materials* 2023; **136**, 109986.

[40] H Gomaa, C An, Q Deng, HA Altaleb, SM Gomha, TZ Abolibda, MA Shenashen and N Hu. A hybrid mesoporous sheet-like $NiCo_2O_4$@P,S,N-doped carbon nano-photocatalyst for efficient synergistic degradation of Congo red: Statistical, DFT and mechanism studies. *Journal of Industrial and Engineering Chemistry* 2025; **141**, 130-144.

[41] F Riyanti, PL Hariani, H Hasanudin, A Rachmat and W Purwaningrum. Optimization photodegradation of methylene blue dye using bentonite/PDA/Fe_3O_4@CuO composite by response surface methodology. *Bulletin of Chemical Reaction Engineering and Catalysis* 2024; **19(2)**, 252-264.

[42] M Shaban, MR Abukhadra, A Hamd, RR Amin and AA Khalek. Photocatalytic removal of Congo red dye using MCM-48/Ni_2O_3 composite synthesized based on silica gel extracted from rice husk ash; fabrication and application. *Journal of Environmental Management* 2017; **204(1)**, 189-199.

[43] MR Dustgeer, A Jilani, MO Ansari, MB Shakoor, S Ali, A Imtiaz, HS Zakria and MHD Othman. Reduced graphene oxide supported polyaniline/ copper (II) oxide nanostructures for enhanced photocatalytic degradation of Congo red and hydrogen production from water. *Journal of Water Process Engineering* 2024; **5**, 105053.

[44] N Kousar, S Rasheed, K Yasmeen, AR Umar, MH Laiche, M Masood, H Muhammad and M Hanif. Efficient synergistic degradation of Congo red and omeprazole in wastewater using rGO/Ag@ZnO nanocomposite. *Journal of Water Process Engineering* 2024; **58**, 104775.

[45] V Arumugaperumal and K Sadaiyandi. Solar light driven photocatalytic degradation of methylene blue dye over Cu doped α-MnO_2 nanoparticles. *Chemical Physics Impact* 2024; **8**, 100434.

[46] MN Aditya, T Chellapandi, GK Prasad, MJP Venkatesh, MMR Khan, G Madhumitha and SM Roopan. Biosynthesis of rod shaped Gd_2O_3 on g-C_3N_4 as nanocomposite for visible light mediated photocatalytic degradation of pollutants and RSM optimization. *Diamond and Related Materials* 2022; **121**, 108790.

[47] S Moosavi, RYM Li, CW Lai, Y Yusof, S Gan, O Akbarzadeh, ZZ Chowhury, XG Yue and MRB Johan. Methylene blue dye photocatalytic degradation over synthesised Fe_3O_4/AC/TiO_2 nano-catalyst: Degradation and reusability studies. *Nanomaterials* 2020; **10(12)**, 2360.